Three-dimensional cardiac magnetic resonance allows the identification of slow-conducting anatomical isthmuses in tetralogy of Fallot

Kimura, Y.; Wallet, J.; Bouyer, B.; Jongbloed, M.R.M.; Bertels, R.; Hazekamp, M.G.; ... ; Zeppenfeld, K.

ESC European Society of Cardiology

European Heart Journal (2024) **45**, 2079–2094
https://doi.org/10.1093/eurheartj/ehae268

CLINICAL RESEARCH
Congenital heart disease

Three-dimensional cardiac magnetic resonance allows the identification of slow-conducting anatomical isthmuses in tetralogy of Fallot

Yoshitaka Kimura [1,2], Justin Wallet [1,2], Benjamin Bouyer [4], Monique R. M. Jongbloed [1,3,5], Robin Bertels [3,6], Mark G. Hazekamp [3,7], Jean-Benoit Thambo [8], Xavier Iriart [8], Hubert Cochet [9], Frederic Sacher [4], Hildo J. Lamb [10], Nico A. Blom [3,6], and Katja Zeppenfeld [1,2]*

[1]Department of Cardiology, Heart-Lung-Center, Leiden University Medical Center (LUMC), P.O. Box 9600, Leiden 2300 RC, The Netherlands; [2]Willem Einthoven Center of Arrhythmia Research and Management (WECAM), Leiden, The Netherlands, and Aarhus, Denmark; [3]Center for Congenital Heart Disease Amsterdam-Leiden (CAHAL), Leiden, The Netherlands; [4]Department of Cardiac Pacing and Electrophysiology, IHU Liryc, Electrophysiology and Heart Modeling Institute, Bordeaux University Hospital (CHU), Bordeaux, France; [5]Department of Anatomy and Embryology, Leiden University Medical Center, Leiden, The Netherlands; [6]Department of Pediatric Cardiology, Leiden University Medical Center, Leiden, The Netherlands; [7]Department of Cardiothoracic Surgery, Leiden University Medical Center, Leiden, The Netherlands; [8]Department of Congenital Heart Disease, Bordeaux University Hospital, Bordeaux, France; [9]Department of Radiology, Bordeaux University Hospital, Bordeaux, France; and [10]Department of Radiology, Leiden University Medical Center, Leiden, The Netherlands

Received 14 September 2023; revised 14 March 2024; accepted 15 April 2024; online publish-ahead-of-print 15 May 2024

See the editorial comment for this article 'A non-invasive gateway to identifying potential substrates for macro-reentrant ventricular tachycardia in tetralogy of Fallot', by P. Khairy, https://doi.org/10.1093/eurheartj/ehae196.

Abstract

Background and Aims Patients with repaired tetralogy of Fallot remain at risk of life-threatening ventricular tachycardia related to slow-conducting anatomical isthmuses (SCAIs). Preventive ablation of SCAI identified by invasive electroanatomical mapping is increasingly performed. This study aimed to non-invasively identify SCAI using 3D late gadolinium enhancement cardiac magnetic resonance (3D-LGE-CMR).

Methods Consecutive tetralogy of Fallot patients who underwent right ventricular electroanatomical mapping (RV-EAM) and 3D-LGE-CMR were included. High signal intensity threshold for abnormal myocardium was determined based on direct comparison of bipolar voltages and signal intensity by co-registration of RV-EAM with 3D-LGE-CMR. The diagnostic performance of 3D-LGE-CMR to non-invasively identify SCAI was determined, validated in a second cohort, and compared with the discriminative ability of proposed risk scores.

Results The derivation cohort consisted of 48 (34 ± 16 years) and the validation cohort of 53 patients (36 ± 18 years). In the derivation cohort, 78 of 107 anatomical isthmuses (AIs) identified by EAM were normal-conducting AI, 22 were SCAI, and 7 blocked AI. High signal intensity threshold was 42% of the maximal signal intensity. The sensitivity and specificity of 3D-LGE-CMR for identifying SCAI or blocked AI were 100% and 90%, respectively. In the validation cohort, 85 of 124 AIs were normal-conducting AI, 36 were SCAI, and 3 blocked AI. The sensitivity and specificity of 3D-LGE-CMR were 95% and 91%, respectively. All risk scores showed an at best modest performance to identify SCAI (area under the curve ≤ .68).

Conclusions 3D late gadolinium enhancement cardiac magnetic resonance can identify SCAI with excellent accuracy and may refine non-invasive risk stratification and patient selection for invasive EAM in tetralogy of Fallot.

* Corresponding author. Tel: +31715262020, Email: K.Zeppenfeld@lumc.nl

Structured Graphical Abstract

Key Question

In repaired tetralogy of Fallot (rTOF), identification of slow conducting anatomical isthmus (SCAI), which predisposes to severe ventricular arrhythmias and sudden death, requires invasive electroanatomical mapping (EAM). 3D late gadolinium enhancement cardiac magnetic resonance (3D-LGE-CMR) may identify SCAI, contributing to individualized risk stratification, treatment planning, and non-invasive follow-up.

Key Finding

In the derivation cohort, 3D-LGE-CMR identified SCAI with excellent sensitivity and specificity (100% and 90%, respectively), which was confirmed in the validation cohort (95% and 91%, respectively).

Take Home Message

3D-LGE-CMR can identify SCAI with excellent accuracy, reducing the need for invasive EAM procedures by about 70%. Thus, 3D-LGE-CMR may improve patient selection for invasive EAM as compared to previously proposed risk scores, characterized by lower predictive accuracy.

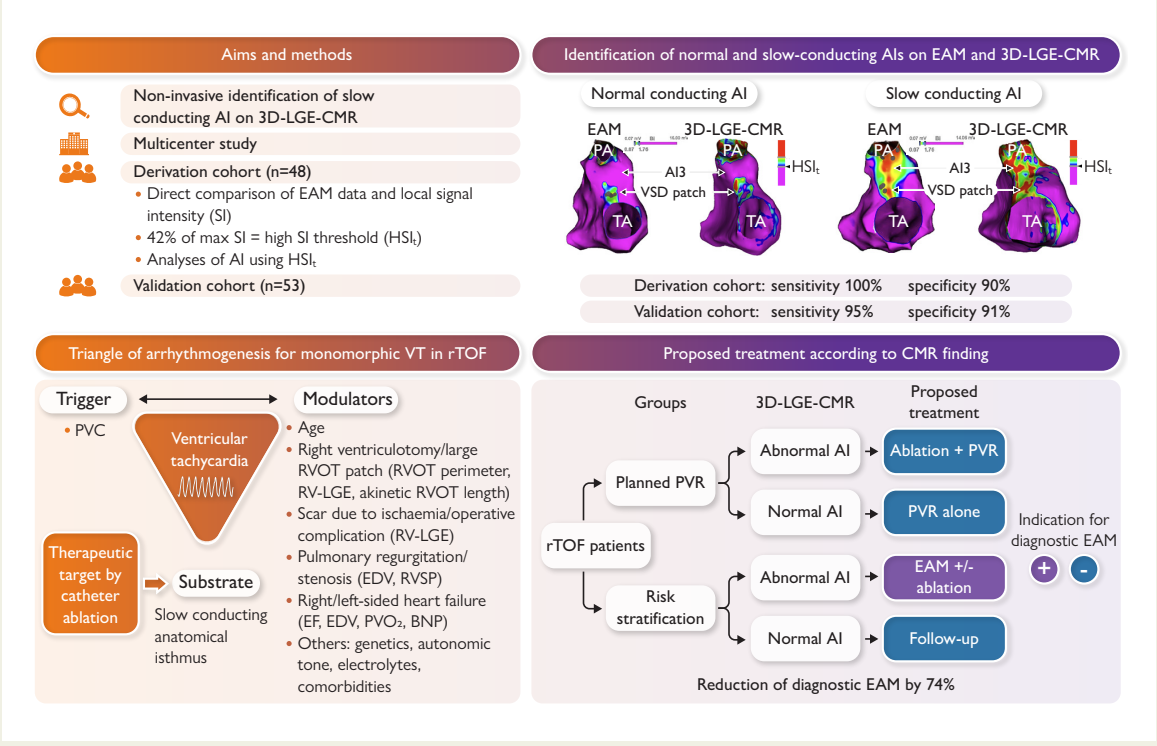

Consecutive rTOF patients with EAM and 3D-LGE-CMR at two centers were included. In the derivation cohort, 3D-LGE-CMR identified SCAI with excellent sensitivity and specificity, which was confirmed in the validation cohort. The occurrence of spontaneous VT depends on the interplay between a pre-existing substrate, initiating triggers and modulating factors (triangle of arrhythmogenesis). 3D-LGE-CMR can significantly reduce the need for diagnostic EAM procedures. AI, anatomical isthmus; BNP, b-type natriuretic peptide; EAM, electroanatomical mapping; EDV, end-diastolic volume; EF, ejection fraction; HSIt, High signal intensity threshold; LGE-CMR, late gadolinium enhancement cardiac magnetic resonance; PVC, premature ventricular complex; PVO2, peak oxygen uptake; PVR, pulmonary valve replacement; rTOF, repaired tetralogy of Fallot; RVOT, right ventricular outflow tract; RVSP, right ventricular systolic pressure; SCAI, slow conducting anatomical isthmus; SI, signal intensity; VT, ventricular tachycardia.

Keywords Tetralogy of Fallot • Ventricular tachycardia • Cardiac magnetic resonance • Anatomical isthmus • Risk stratification

Introduction

Advances in surgical repair and medical treatment have improved survival in patients with tetralogy of Fallot (TOF).[1,2] The risk of sudden cardiac death (SCD) due to sustained monomorphic ventricular tachycardia (SMVT) remains of concern.

The vast majority of documented ventricular arrhythmias (VAs) in repaired TOF (rTOF) are SMVT due to re-entry. The critical component of the re-entry circuit is typically located within anatomically defined isthmuses (AIs) bordered by unexcitable structures such as surgical scars, patches, and valve annuli. While AIs are present in almost all rTOF patients, only those with abnormal myocardium leading to

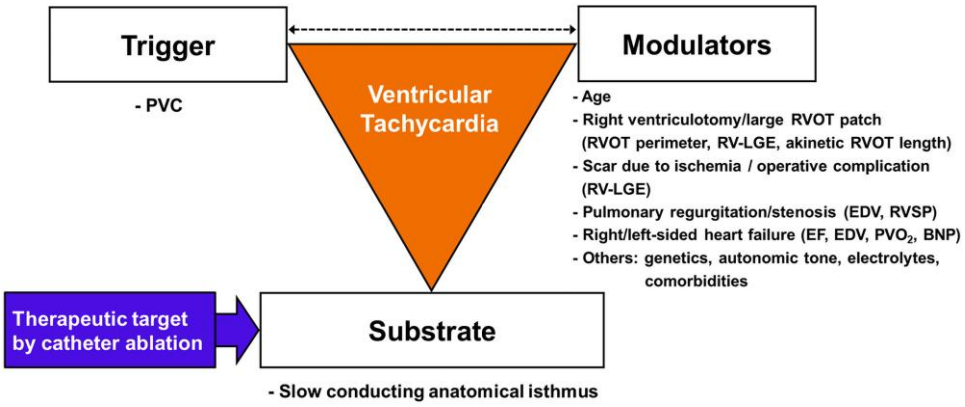

Figure 1 Triangle of arrhythmogenesis for monomorphic ventricular tachycardia in patients with repaired tetralogy of Fallot. BNP, B-type natriuretic peptide; EDV, end-diastolic volume; LGE, late gadolinium enhancement; LVEF, left ventricular ejection fraction; PVC, premature ventricular complex; PVO_2, peak oxygen uptake; PVR, pulmonary valve replacement; RVEF, right ventricular ejection fraction; RVOT, right ventricular outflow tract; RVSP, right ventricular systolic pressure

slow-conducting properties during baseline rhythm [slow-conducting AI (SCAI), conduction velocity (CV) < .5 m/s during sinus rhythm (SR)] are arrhythmogenic and play a key role for re-entry SMVT.[3–6]

Patients without SCAI or after successful transection of SCAI by catheter ablation have excellent ventricular tachycardia (VT)-free survival,[7] while patients with a SCAI not successfully ablated or not targeted remain at risk for SMVT.[5] Of note, the abnormal myocardium of SCAI may not be longer accessible by catheter ablation after surgical or percutaneous pulmonary valve replacement (PVR),[8–10] accordingly preventive ablation of SCAI before PVR is increasingly performed.[10–15] Time- and disease-dependent modulating factors, including age and residual or new haemodynamical lesions, and initiating triggers may contribute to arrhythmogenesis and the occurrence of spontaneous SMVT in rTOF patients with a pre-existing SCAI (triangle of arrhythmogenesis; *Figure 1*). This interaction may further support preventive ablation of SCAI before spontaneous VT has occurred.[10–13,15–17] Several risk scores have been developed to predict adverse outcome in rTOF,[18–21] while their performance to predict the presence of SCAI has not been evaluated. Currently, the identification of SCAI requires invasive electroanatomical mapping (EAM). As slow conduction may develop over time, repeated EAM may be required.

Compared with 2D late gadolinium enhancement cardiac magnetic resonance (LGE-CMR), 3D-LGE-CMR allows accurate visualization of morphologically complex parts of the heart such as the right ventricular (RV) outflow tract (RVOT) with high spatial resolution.[22] Non-invasive identification of SCAI by LGE-CMR has not been achieved but may significantly contribute to individualized risk stratification and non-invasive follow-up.

In the present study, we aimed to (i) determine rTOF-specific signal intensity (SI) threshold values to identify abnormal myocardium by 3D registration of LGE-CMR and EAM; (ii) assess the performance of 3D-LGE-CMR to non-invasively identify SCAI; and (iii) compare this with the performance of previously proposed risk scores[18–21] to non-invasively identify SCAI.

Methods

Study population and study design

Consecutive patients with rTOF who underwent RV-EAM and 3D-LGE-CMR at Leiden University Medical Center (LUMC), the Netherlands (September 2012 to June 2023, $n = 61$) and Bordeaux University Hospital (CHU), Bordeaux, France (August 2010 to October 2018, $n = 40$) were included. Electroanatomical mapping was performed before ablation in patients presenting with VT or out-of-hospital cardiac arrest, prior to planned surgical PVR, or as part of risk stratification according to the standard clinical protocol.[5] Patients were assigned to the derivation or validation cohort according to procedure date and including institution (see Supplementary data online, *Method S1*).

All patients provided informed consent for the procedure. The protocol applies to the Declaration of Helsinki and was approved by the internal review board of the cardiology department in the LUMC. For the retrospective part, the Medical Ethics Committee (METC Leiden Den Haag Delft) waived the need for written informed consent, as all data were acquired according to routine clinical care. The prospective registry was approved by the METC (G21.137).

Baseline evaluation

A comprehensive clinical evaluation was performed before EAM. Medical records were reviewed for the details of prior surgeries and for documented VA. QRS duration, morphology, and fragmented QRS were assessed on non-paced 12-lead electrocardiographies. Fragmented QRS was defined as previously described.[20] Blood sampling for N-terminal pro-B-type natriuretic peptide and cardiopulmonary exercise testing were performed if clinically indicated. Peak oxygen uptake was included when the respiratory exchange ratio was >1.

Biventricular systolic function and pulmonary valve insufficiency were measured with CMR. The left and RV functions were classified as severely reduced (<30%), moderately reduced (30%–39%), mildly reduced (40%–54%), or good (≥55%).[7] Right ventricular systolic pressure (RVSP) and left ventricular (LV) diastolic dysfunction (LVDD) were assessed by transthoracic echocardiography, and LVDD was defined as mitral lateral $e' <$ 10 cm/s and E/e' ratio ≥ 9.[23,24]

3D late gadolinium enhancement cardiac magnetic resonance acquisition and processing

Cardiac magnetic resonance examinations in the LUMC were performed on a 1.5 T Gyroscan ACS-NT/Intera MR system or on a 3.0 T Ingenia MR system (Philips Medical Systems, Best, the Netherlands).[25] Following a standardized clinical protocol including cine magnetic resonance imaging in long axis (two- and four-chamber views) and short axis, the gadolinium-based contrast agent (Dotarem, Guerbet, Villepinte, France) was given intravenously (dosage, .15 mmol/kg). Ten minutes after contrast administration, a 2D gradient-echo T1-weighted sequence was used to visually determine the optimal inversion time (T1) of healthy myocardium. Approximately 10–15 min after administration of contrast, a whole heart

high spatial resolution 3D gradient echo (T1 fast field echo) phase-sensitive inversion recovery (PSIR) sequence was obtained during free breathing with diaphragmatic pencil-beam navigation (see Supplementary data online, *Method S2*). Typical parameters were as follows: repetition time 4.15 ms; echo time 2.02 ms; the optimal inversion time was set at the null point plus 50 ms and ranged from 250 to 400 ms; flip angle 10°; field of view 350 × 350 mm; matrix size 208 × 208; acquired pixel size 1.68 × 1.68 mm; reconstructed pixel size .91 × .91 mm; 71 transverse slices with 3.4 mm thickness and slice gap −1.7 mm; and sensitivity encoding factor 3. Immediately after free-breathing LGE-CMR, breath hold was obtained using a 3D gradient echo PSIR sequence in short-axis slice orientation in two equal stacks during two breath holds of 10- to 20-s duration. The detailed description of the MRI protocol in CHU can be found in Supplementary data online, *Method S3*.

Risk scores

Five previously published risk scores, which included[18,21] or not included LGE-CMR parameters[19,20] to predict adverse outcomes in patients with rTOF, were calculated for each patient (see Supplementary data online, *Method S4*).

Electrophysiology study and electroanatomical mapping

Programmed electrical stimulation (PES) was performed from the RV apex and the RVOT, at or adjacent to the infundibular septum with up to four drive-cycle lengths (CLs: 600, 500, 400, and 350 ms) and up to four extra stimuli, until the ventricular effective refractory period or a minimum coupling interval of 200 ms (180 ms in patients ≤ 18 years old) was reached. The protocol was repeated after administration of isoproterenol if necessary. Sustained monomorphic ventricular tachycardia was defined as VT with a similar QRS configuration from beat to beat, lasting ≥30 s or causing haemodynamic compromise requiring termination. The detailed methods to obtain a 3D reconstruction of all four AIs and to target the VT-related isthmus by ablation have been previously reported.[3,5,11,17,26] The potential four AIs and their anatomical boundaries are illustrated in *Figure 2A*.

Briefly, 3D-RV (and LV and aorta if necessary) electroanatomical bipolar voltage (BV) mapping during baseline rhythm was performed using a 3.5 mm irrigated-tip catheter (NaviStar Thermocool, Smarttouch, Biosense Webster Inc., Irvine, CA, USA) and long steerable sheaths. The aorta and LV were approached by retrograde access. The locations of the tricuspid annulus (TA) and pulmonary annulus (PA) and unexcitable tissue (patch material) were determined by the local electrograms (EGMs) and/or non-capturing by pacing at 10 mA/2 ms.

After completing RV mapping, the entrance and exit sites of the AI were determined to measure AI length and to determine the conduction time through each AI. For this purpose, sites with the first normal configurated bipolar EGM (≤4 deflections without fractionations or late components, typically with BV > 1.5 mV) at each site of an AI were selected, and the local activation times at these sites were assessed based on the downstroke of the corresponding unipolar EGM. Anatomical isthmus length and conduction time were determined by measuring the distance using the software of the 3D mapping system (CARTO 3™) and by calculating the difference in local activation time between entrance and exit sites, respectively (*Figure 2B and E*).[5] In cases with QRS duration < 150 ms and/or colliding activation wavefronts within an AI during non-paced rhythm, the RV was re-mapped during pacing from the septal or lateral site of the isthmus just above SR rate to allow correct determination of the conduction time.[27] If the calculated CV (distance/time) across the AI was <.5 m/s, the AI was considered SCAI,[5] and an AI with CV ≥ .5 m/s was considered as normal-conducting AI (NCAI). A blocked AI was defined as AI with pre-existing bidirectional conduction block.[26] The analyses of EAM were performed by at least two operators in each centre.

Ablation and follow-up

Ablation of a SCAI was considered successful if conduction through SCAI was bidirectionally blocked after radiofrequency delivery. In selected patients in whom PVR was planned, intraoperative cryoablation of the VT-related AI was performed, with intraoperative confirmation of bidirectional conduction block.[12]

Patients were followed according to institutional protocols (see Supplementary data online, *Method S5*).

Late gadolinium enhancement cardiac magnetic resonance-derived 3D scar reconstructions and evaluation of anatomical isthmuses

Late gadolinium enhancement images in DICOM format were imported to the ADAS-3D image post-processing software tool (Galgo Medical, Barcelona, Spain). The RV wall was traced semi-automatically and then manually corrected for a mid-myocardial layer while ensuring the avoidance of artefacts from sternal wire/prosthetic valves and high-intensity signal from the blood pool (*Figure 3A*).[28] The maximum and minimum voxel SIs (MaxSI and MinSI) on the 3D-RV-shell were automatically detected and exported.

Next, the obtained 3D-LGE-CMR-derived RV reconstruction was merged with the 3D-RV CARTO mesh file. For registration, the TA, ventricular septal defect patch, PA, and RV apex were used as landmarks utilizing ADAS-3D software. After visual assessment, additional anatomical structures (i.e. pulmonary artery and RV septum) were used to optimize registration. Electroanatomical mapping points were superimposed on the CMR-derived reconstruction, which allows for direct comparison of EAM data and local SI. Electroanatomical mapping points > 10 mm away from the CMR-derived reconstruction were removed from the analysis (*Figure 3B*).

The percentage of MaxSI (%MaxSI) at each EAM site was calculated for each EAM point by the equation: %MaxSI = (Local SI − MinSI)/(MaxSI − MinSI) ∗ 100.

Data on BV and %MaxSI for each EAM point were retrieved in all patients. The optimal threshold of %MaxSI to detect abnormal low BV (threshold < 1.76 mV based on previously published normal BV data using contact force sensing catheters in the RV in patients with rTOF)[29] was determined by receiver operating characteristic (ROC) analysis. The obtained high SI threshold (HSI_t) was applied to the CMR-derived 3D-RV reconstruction, colour coded for the local %MaxSI (*Figure 3C*). Of note, BV < 1.76 mV indicates any diseased myocardium, including but not restricted to unexcitable tissue. Accordingly, myocardium with a SI above the HSI_t includes both unexcitable boundaries and diseased myocardium with slow-conducting properties.

All AIs on the 3D-LGE-CMR-derived reconstruction were analysed. An abnormal AI on CMR was defined as AI showing continuous high SI (>HSI_t) connecting the anatomical boundaries; otherwise, an AI was considered normal. In cases of a normal AI on 3D-CMR reconstruction, the minimal width of the normal SI area between the two anatomical boundaries was measured using a tool deployed to the software (*Figure 3C*). Total RV surface area and the area with SI above the HSI_t were automatically calculated.

For the derivation cohort, all CMR analyses were performed by an experienced operator blinded to EAM data. To assess inter-observer reproducibility, 20 cases were re-analysed by a second operator, and the total RV surface area, the area above the HSI_t, and the presence of abnormal AI on CMR were compared. For the validation cohort, all analyses were performed by two experienced operators blinded to EAM data.

Statistical analysis

Continuous data are presented as mean ± SD or median [interquartile range (IQR)] according to distribution. Categorical data are reported as percentage and frequency. Continuous variables were compared using the Student's *t*-test or the Mann–Whitney *U* test where appropriate. Categorical variables were compared using the chi-square test. Odds ratios of clinical parameters and risk scores for the presence of SCAI or blocked AI (SCAI/blocked AI) and VT inducibility were calculated using univariable logistic regression analysis. The performance of risk scores to predict the presence of SCAI/blocked AI and VT inducibility was determined using ROC curves. Patients who had undergone ablation of AI before CMR were not included in the univariable logistic regression analysis or the

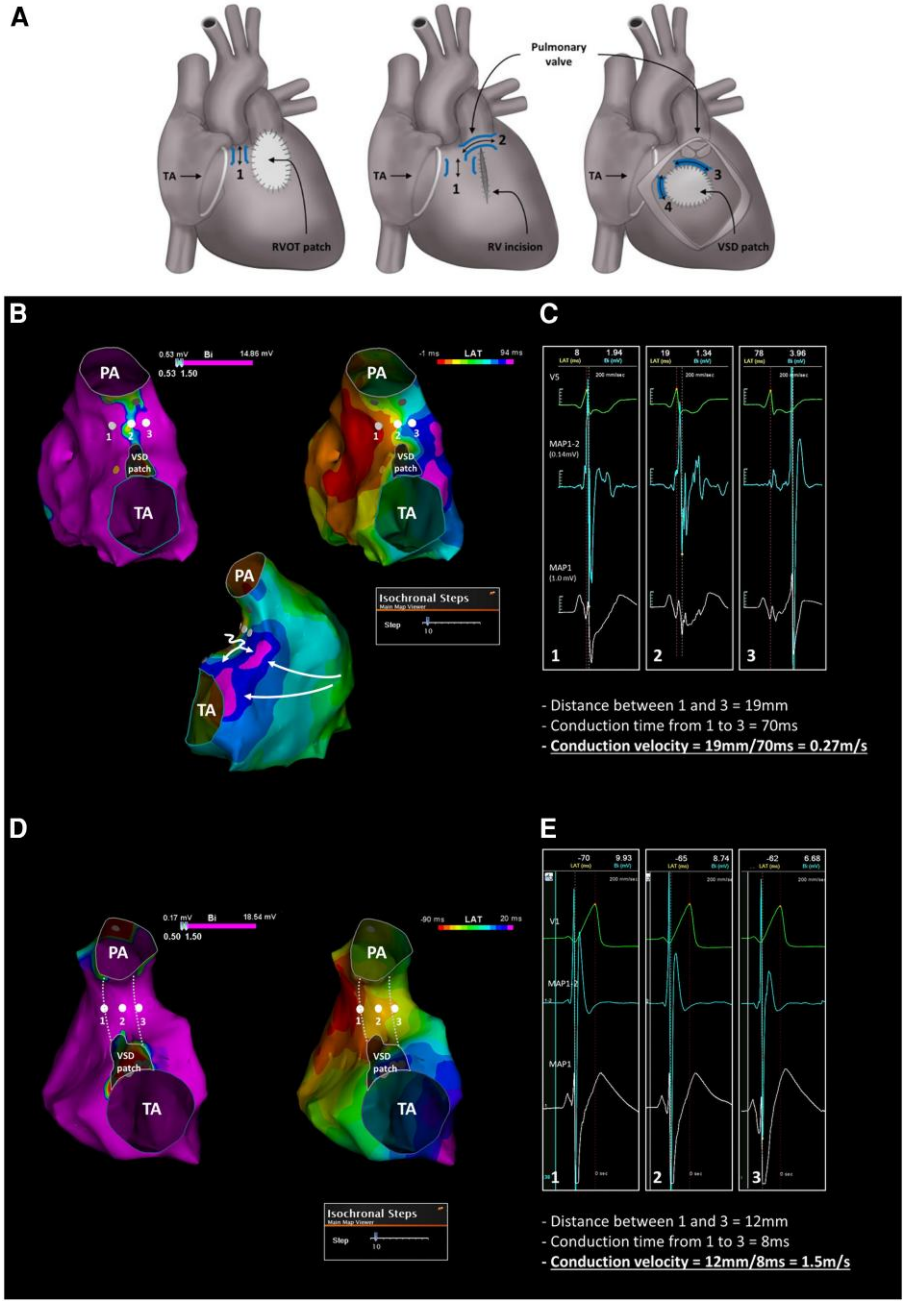

Figure 2 Electroanatomical evaluation of anatomical isthmus. (*A*) Schematic overview of the four potential anatomical isthmuses. Anatomical isthmus 1 is located between the tricuspid annulus and the right ventricular outflow tract patch/right ventricular incision. Anatomical isthmus 2 is bordered by an RV incision and the pulmonary annulus, and its presence depends on the type of surgical approach. Anatomical isthmuses 3 and 4 are located at the infundibular septum, with anatomical isthmus 3 between pulmonary valve and ventricular septal defect patch, and anatomical isthmus 4 between ventricular septal defect patch and tricuspid annulus in case of muscular ventricular septal defect. Adapted from Kapel *et al.*[5] with permission by Oxford University Press. (*B* and *C*) Slow-conducting anatomical isthmus 3. (*B*) (Upper left panel) modified posterior view showing anatomical isthmus 3 bordered by the ventricular septal defect patch and the pulmonary annulus. Bipolar voltages are colour coded according to bar, voltage > 1.5 mV (purple), grey tags indicate sites with no capture at high output pacing (10 mA/2 ms) consistent with scar/prosthetic material. The yellow tag represents the site where a His electrogram was recorded. The local electrograms in and at both sides of AI3, corresponding to electrograms 1, 2, and 3 are shown in *C*. (Upper right panel) the same map is displayed as an activation map. Local activation time is colour coded according to bar. A broad area of early activation is evident at the septum (typical for right bundle branch block [RBBB]) and late activation at the posterolateral right ventricle. Based on the local signal characteristics, normal (non-fragmented) bipolar electrogram sites at the entrance of anatomical isthmus 3 (Site 1) and the exit of anatomical isthmus 3 (Site 3) were selected, allowing for accurate determination of the local activation time based on the downstroke of the unipolar electrogram recorded from the tip of the mapping catheter. The length of anatomical isthmus 3 (19 mm) is measured as the distance between the selected entrance

Continued

ROC curve analysis. The intra-class correlation coefficient was used to determine inter-observer variabilities in total RV surface area, total scar area, and percentage of total scar area on CMR, and Kappa coefficient was calculated for agreement on the presence of abnormal AI on CMR. All tests were two-sided, and a *P*-value of <.05 was considered statistically significant. All analyses were performed with SPSS 25.0 (IBM Corporation, Armonk, NY, USA).

Results

Derivation cohort

Forty-eight patients were included (34 ± 16 years, 58% male) in the derivation cohort (*Table 1*). Five patients (10%) underwent EAM for spontaneous VT, 19 patients (40%) before PVR, and the remaining 24 patients (50%) for risk stratification (see Supplementary data online, *Table S1*). The median age at initial repair was 2.6 (IQR .7–6.2) years. The mean QRS duration was 155 ± 30 ms. Cardiac magnetic resonance was performed at a median of 55 days (IQR 2–154) before EAM. Mean LVEF and RVEF were 55 ± 7% and 48 ± 8%, respectively.

Electrophysiological study and electroanatomical mapping data

A total of 107 AIs were identified on EAM. Anatomical isthmuses 1 and 3 were present in all patients, while AI2 was identified in 11 patients (23%) and AI4 in none (*Table 2*). All AI1 had normal CV. Slow-conducting anatomical isthmuses 2 and 3 were observed in 2 (4%) and 20 patients (42%), respectively. Seven patients (15%) had a blocked AI3, including three after previous ablation. The remaining 78 AIs were NCAI.

In 11 patients, 14 SMVTs (median CL 250 ms; IQR 231–278 ms) were induced, all related to SCAI3.

Association between non-invasive parameters, risk scores, and the presence of slow-conducting anatomical isthmus/ blocked anatomical isthmus

In univariable analysis of clinical parameters, only the presence of transventricular repair was significantly associated with the presence of SCAI/blocked AI (*Table 3*). Among previously published risk scores, only the score by Babu-Narayan *et al.* showed a significant correlation, with an area under the curve (AUC) of .65 (*Table 4*). None of the risk scores could exclude patients with SCAI/blocked AI, based on a low score or on the presence of only minimal/mild RV-LGE (*Figure 4*).

Association between non-invasive parameters, risk scores, and ventricular tachycardia inducibility

In univariable analysis, palliative shunt operation, transventricular repair, and LVEF were significantly associated with VT inducibility (see Supplementary data online, *Table S2*). Among the available risk scores, only those including RV-LGE[18,21] showed a good discriminative ability for VT inducibility (AUC of .86 and .80, respectively; Supplementary data online, *Table S3*). These two risk scores could identify non-inducible patients, based on a low score or the presence of only minimal/mild RV-LGE (see Supplementary data online, *Figure S1*).

Reversed registration of bipolar voltage mapping data and 3D late gadolinium enhancement cardiac magnetic resonance-derived right ventricular reconstruction

A total of 10 178 mapping points were superimposed onto the 3D-CMR RV reconstruction, and 9240 points within 10 mm from the 3D-CMR RV reconstruction were used for the analysis. There was a significant inverse relationship between local BV and %maxSI ($R^2 = .16$, $P < .001$; *Figure 5A*). Based on ROC curve analysis, HSI_t to detect abnormal low BV (<1.76 mV) was 42% of the maximal SI with a sensitivity of 74% and a specificity of 78% (AUC .80; *Figure 5B*).

Identification of slow-conducting anatomical isthmus by 3D cardiac magnetic resonance reconstruction using the disease-specific signal intensity threshold for low bipolar voltage

Using the HSI_t (42% of maxSI), 3D-CMR reconstructions were analysed. Representative two cases are illustrated in *Figure 6*. The total

Figure 2 Continued
and exit sites (1 and 3) using the software of the 3D mapping system. (Lower panel) Modified right lateral view showing the latest local activation time site in the right ventricle to ensure that the activation wavefronts from the septal and lateral right ventricle do not collide within anatomical isthmus 3. If such collision occurs, remapping during pacing near anatomical isthmus 3 is necessary to accurately measure the conduction time through anatomical isthmus 3. (*C*) Local electrograms in and at both sides of anatomical isthmus 3. The difference between the local activation time at the entrance (Site 1, 8 ms) and exit (Site 3, 78 ms) sites determines the conduction time through the anatomical isthmus, which is 70 ms. Using the anatomical isthmus length and conduction time, the conduction velocity can be calculated (19 mm/70 ms = .27 m/s), which is abnormal. In this patient, anatomical isthmus 3 was the only slow-conducting anatomical isthmus and related to the ventricular tachycardia. (*D* and *E*) Normal-conducting anatomical isthmus 3. (*D*) (Left panel) modified posterior view showing anatomical isthmus 3. Bipolar voltages are colour coded according to bar, voltage ≥ 1.5 mV (purple). The local electrograms in and at both sides of anatomical isthmus 3 corresponding to electrograms 1, 2, and 3 are shown in *E*. In this case, bipolar voltage is consistently >1.5 mV throughout the anatomical isthmus 3. The entrance and exit of anatomical isthmus 3 (Sites 1 and 3) are determined by lines extending from the septal and lateral extension of the ventricular septal defect patch to the pulmonary annulus, as indicated by dashed lines. (Right panel) the same map is displayed as an activation map. Local activation time is colour coded according to bar, showing a broad area of early activation at the septum and late activation at the inferolateral right ventricle. At two sites at the entrance of anatomical isthmus 3 (Site 1) and the exit of anatomical isthmus 3 (Site 3), the local activation time is determined based on the downstroke of the unipolar electrogram recorded from the tip of the mapping catheter. The length of anatomical isthmus 3 (12 mm) is the distance between Sites 1 and 3. (*E*) Local electrograms in and at both sides of anatomical isthmus 3. The conduction time through the anatomical isthmus 3 is 8 ms. Accordingly, the conduction velocity can be calculated (12 mm/8 ms = 1.5 m/s), which is normal. PA, pulmonary annulus; TA, tricuspid annulus

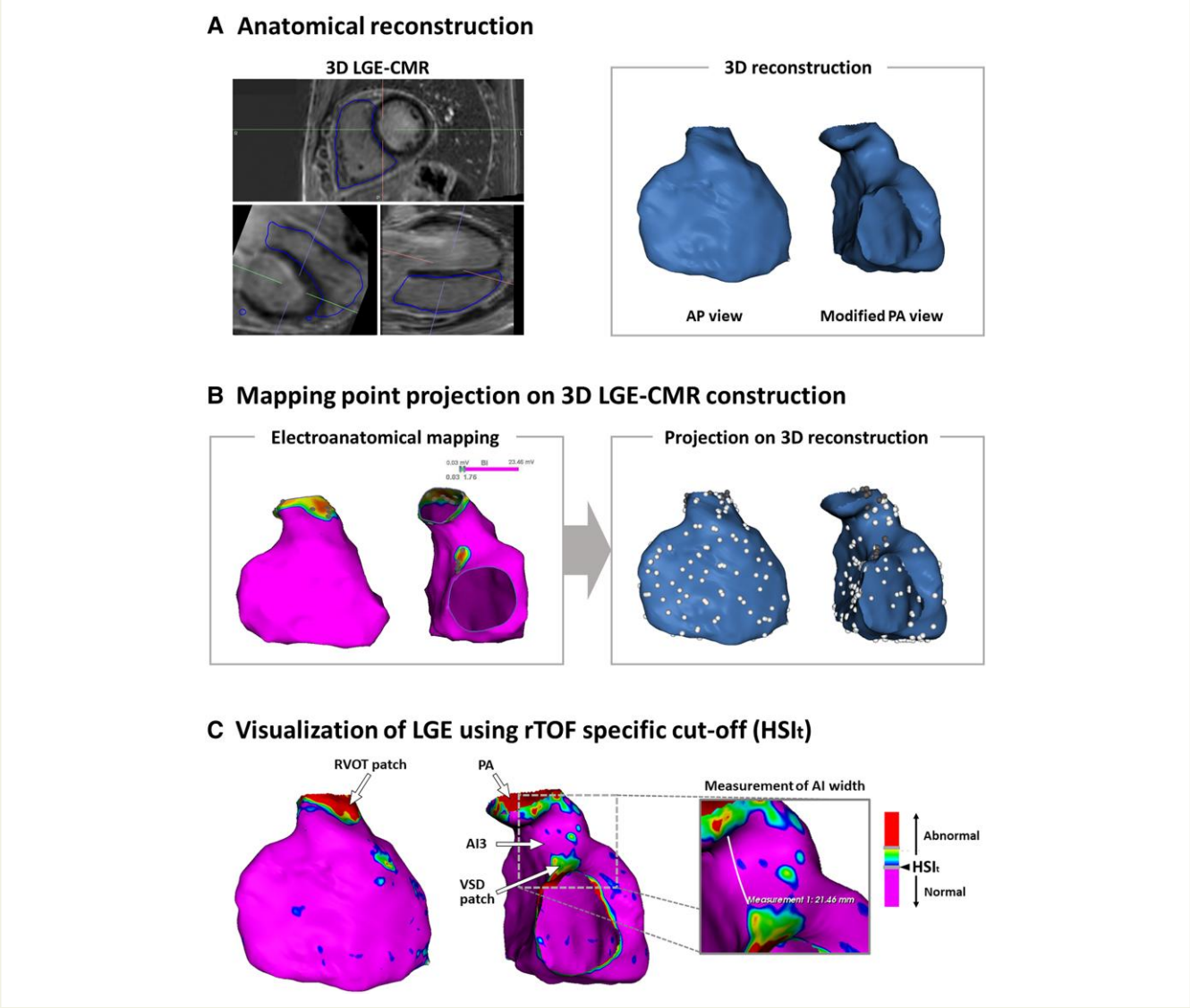

Figure 3 Processing of 3D late gadolinium enhancement cardiac magnetic resonance and integration with electroanatomical map. (*A*) (Left panel) right ventricular contour was semi-automatically traced and manually corrected for a mid-myocardial layer. Noises by sternum wire were carefully removed from the contour. (Right panel) Tricuspid valve and pulmonary artery were removed from the 3D late gadolinium enhancement cardiac magnetic resonance reconstruction. The imaging processing software automatically detects the maximum and minimum signal intensities of the 3D late gadolinium enhancement cardiac magnetic resonance reconstruction. (*B*) (Left panel) right ventricular electroanatomical mapping was reviewed and exported. (Right panel) All mapping points were superimposed onto the 3D late gadolinium enhancement cardiac magnetic resonance reconstruction. Electroanatomical mapping points > 10 mm away from the cardiac magnetic resonance-derived reconstruction were removed from the analysis, and bipolar voltage of the remaining points was compared with corresponding local signal intensities (see *Figure 2*). (*C*) (Left and mid panels) the obtained high signal intensity threshold (42% of the maximum signal intensity) was applied to the 3D cardiac magnetic resonance right ventricular reconstruction, visualizing the right ventricular shell colour coded by local percentage of MaxSI and the scar lesion defined as an area above the high signal intensity threshold. An additional threshold was put at 1.5-fold of the high signal intensity threshold but not used for analysis. Abnormal myocardium (>HSI_t) was visualized as red, yellow, green, or blue, and normal myocardium (<HSI_t) was as purple. Anatomical isthmuses on the 3D late gadolinium enhancement cardiac magnetic resonance-derived construction were visually inspected if it is abnormal anatomical isthmus, defined as a continuous area above the high signal intensity threshold connecting anatomical boundaries. (Right panel) in cases with a normal anatomical isthmus on cardiac magnetic resonance, the lesion width of the healthy part of the anatomical isthmus was measured using a tool deployed to the software. AI, anatomical isthmus; BV, bipolar voltage; CMR, cardiac magnetic resonance imaging; EAM, electroanatomical mapping; HSI_t, high signal intensity threshold; LGE, late gadolinium enhancement; RV, right ventricle; SI, signal intensity

RV surface area and the area > HSI_t were 238 ± 44 and 55 ± 25 cm^2, respectively. All unexcitable boundaries of AI as identified by EAM, including patch materials, incision, and at least a part of valve annuli had a SI above the HSI_t.

Of the 107 AI, 37 AI in 33 patients were categorized as abnormal AI based on 3D-LGE-CMR (*Table 2*). Importantly, all 29 SCAI/blocked AI on EAM were correctly classified as abnormal AI on CMR. Among the 78 NCAI, 70 were correctly categorized as normal AI on CMR.

Table 1 Baseline data of the derivation cohort

	Derivation cohort ($n = 48$)
Age, years	34 ± 16
Male sex	28 (58)
Initial repair	
Age at total repair, years	2.6 (.7–6.2)
Initial repair ≥ 5 years	17 (35)
Palliative shunt ($n = 46$)	14 (30)
Transannular patch ($n = 47$)	30 (64)
Transventricular repair ($n = 36$)	18 (50)
PVR	23 (45)
Syncope	2 (4)
ECG	
QRS duration, ms	155 ± 30
QRS duration ≥ 180 ms	9 (19)
CRBBB	42 (88)
FQRS	28 (58)
History of atrial arrhythmia	10 (21)
NSVT	17 (38)
Clinical SMVT	5 (10)
LV diastolic dysfunction ($n = 45$)	5 (11)
RVSP, mmHg	35 (26–44)
PVO_2, mL/kg/m^2 ($n = 37$)	26.5 (20.9–31.6)
NT-proBNP, pg/mL ($n = 25$)	168 (68–293)
CMR	
LVEF, %	55 ± 7
RVEF, %	48 ± 8
LVEF good/mildly reduced	48 (100)
RVEF good/mildly reduced	42 (87)
RVEDV, mL	227 ± 61
RVEDVI, mL/m^2	128 ± 34
PR moderate/severe	23 (48)

Results are expressed as a number (%), mean ± SD, or median (IQR).
CMR, cardiac magnetic resonance imaging; CRBBB, complete right bundle branch block; ECG, electrocardiography; FQRS, fragmented QRS; LV, left ventricle; LVEF, left ventricular ejection fraction; MRI, magnetic resonance imaging; NSVT, non-sustained ventricular tachycardia; NT-proBNP, N-terminal pro-B-type natriuretic peptide; PR, pulmonary regurgitation; PVO_2, peak oxygen uptake; PVR, pulmonary valve replacement; RV, right ventricle; RVEDV, right ventricular end-diastolic volume; RVEDVI, right ventricular end-diastolic volume index; RVEF, right ventricular ejection fraction; RVSP, right ventricular systolic pressure; SMVT, sustained monomorphic ventricular tachycardia.

The median minimal widths of normal AI2 and AI3 on CMR were 14.6 mm (range 11.3–34.8 mm) and 15.5 mm (range 6.3–27.4 mm), respectively. The remaining 8/78 (10%) NCAI were considered abnormal AI on CMR (*Table 2*).

The sensitivity and specificity of 3D-LGE-CMR for identifying SCAI/blocked AI were 100% and 90% (29/29 and 70/78), respectively. Data for each AI are provided in *Table 2*. The results were similar if patients with previous ablation were excluded (see Supplementary data online, *Table S4*).

Inter-observer variability

Intra-class correlation coefficients were .97 [95% confidence interval (CI) .93–.99] for the total RV surface area and .97 (95% CI .93–.99) for the area with SI > HSI_t. Kappa coefficient was 1.0.

Association between bipolar voltage, conduction velocity, and cardiac magnetic resonance findings of anatomical isthmus 3

Patients were divided into three groups according to the EAM and CMR findings of AI3, considering EAM as the gold standard: (i) NCAI on EAM and normal AI on CMR ('true negative CMR', $n = 15$), (ii) NCAI on EAM and abnormal AI on CMR ('false-positive CMR', $n = 6$), and (iii) SCAI on EAM and abnormal AI on CMR ('true positive CMR', $n = 20$). There were no false negatives.

The median BV and CV of AI3 in all patients were 1.68 (IQR .61–2.62) mV and .64 (.36–.93) m/s, respectively. Of note, the median BV within AI3 was highest in Group A, followed by Groups B and C ($P < .01$ for both A vs. B and B vs. C; *Figure 7A*). In addition, the median CV was highest in Group A, followed by Groups B and C (A vs. B, $P < .01$, B vs. C, $P < .001$; *Figure 7B*).

Acute ablation outcome

All 20 SCAI3 were targeted by radiofrequency ($n = 10$) or surgical cryoablation ($n = 10$), with acute procedural success in 17/20 (85%). The reason for three ablation failures was inaccessibility likely due to prior PVR/artificial material, and an implantable cardioverter-defibrillator (ICD) was implanted in all 3. The two SCAI2 were successfully transected by radiofrequency catheter ablation ($n = 1$) or surgically during PVR ($n = 1$).

Follow-up

During a median follow-up of 25 (IQR 11–45) months, two patients had VT, both with SCAI3 and ablation failure.

In one patient with a normal but narrow (6.3 mm) AI3 on a first CMR and corresponding normal CV through the AI3 (.81 m/s) on EAM, a second 3D-LGE-CMR was performed 4 years later because of palpitations. Cardiac magnetic resonance was consistent with an abnormal AI3, and EAM confirmed a SCAI3, which was the critical substrate for an induced SMVT. Anatomical isthmus 3 was successfully transected by catheter ablation (*Figure 8*).

Validation cohort

Fifty-three patients were included (36 ± 18 years, 81% male) in the validation cohort. The reasons for EAM were clinical VT in 3 (6%), before PVR in 31 (58%), and risk stratification in 19 patients (36%) (see Supplementary data online, *Table S5*). Cardiac magnetic resonance was performed at a median of 38 days (IQR 1–114) before EAM.

A total of 124 AIs were identified on EAM (*Table 5*). Anatomical isthmuses 1 and 3 were present in all patients, while AI2 was identified in 16 patients (30%) and AI4 in 2 (4%). Of 124 AIs, 36 (29%) were SCAI. Three patients (6%) had a blocked AI3, including 2 with previous ablation. The remaining 85 AIs were NCAI.

Table 2 Electroanatomical mapping and cardiac magnetic resonance data of the derivation cohort

		Normal AI_{CMR}	Abnormal AI_{CMR}	Total	Sensitivity (95% CI)	Specificity (95% CI)
$AI_{EAM}1$	NCAI	48	0	48	n/a	100% (93–100)
	SCAI	0	0			
$AI_{EAM}2$	NCAI	7	2	11	100% (16–100)	78% (46–96)
	SCAI	0	2			
$AI_{EAM}3$	NCAI	15	6	48	100% (87–100)	71% (50–88)
	SCAI	0	20			
	Blocked AI	0	7			
$AI_{EAM}4$		0	0	0	n/a	n/a
Total		70	37	107	100% (88–100)	90% (82–95)

95% CI, 95% confidence interval; AI, anatomical isthmus; CMR, cardiac magnetic resonance; EAM, electroanatomical mapping; NCAI, normal-conducting anatomical isthmus; SCAI, slow-conducting anatomical isthmus.

Table 3 Univariable analyses for the presence of slow-conducting anatomical isthmus/blocked anatomical isthmus

	Odds ratio	95% CI	*P*-value
Age, per 1 year	1.03	.99–1.07	.12
Male sex	2.20	.66–7.35	.20
Age at total repair, per 1 year	1.06	.91–1.23	.42
Initial repair ≥ 5 years	1.92	.52–7.05	.32
Palliative shunt	3.64	.82–16.1	.07
Transannular patch	.34	.09–1.24	.09
Transventricular repair	7.15	1.53–33.4	.01
QRS duration, per 1 ms increase	1.02	.99–1.04	.12
FQRS	2.20	.66–7.35	.20
History of atrial arrhythmia	2.50	.43–14.5	.29
NSVT	.67	.19–2.33	.53
RVEF moderate/severely reduced	1.82	.15–21.6	.64
LV diastolic dysfunction	1.00	.13–7.85	1.00
PR moderate/severe	.63	.20–2.06	.45
LVEF, per 1% increase	.96	.88–1.05	.33
RVEF, per 1% increase	1.00	.93–1.08	.98
Area > HSI_t, per 1 cm^2 increase	1.03	1.00–1.06	.04

CI, confidence interval; HSI_t, high signal intensity threshold.
See *Table 1* for other abbreviations.

All but two SCAI/blocked AI on EAM were correctly classified as abnormal AI on CMR (*Table 5*). Reconstructed CMR images of the two cases with false-negative CMR findings (SCAI on EAM but normal AI on CMR) are shown in Supplementary data online, *Figure S2*. Among the 85 NCAI on EAM, 77 were correctly categorized as normal AI on CMR, and 8 (9%) were considered as abnormal AI on CMR.

The sensitivity and specificity of 3D-LGE-CMR for identifying SCAI/blocked AI were 95% and 91% (30/32 and 77/85), respectively (*Table 5*). The results were similar if patients with previous ablation were excluded (see Supplementary data online, *Table S6*).

Potential impact of systematic evaluation by cardiac magnetic resonance on indication for electroanatomical mapping in patients without spontaneous ventricular tachycardia or previous ablation

In the entire cohort ($n = 101$), 88 patients had no previous spontaneous VT or prior ablation. Of those, 48 patients (19 derivation and 29 validation cohort) underwent EAM for evaluation before PVR, showing at least one abnormal AI on CMR in 32 patients and only normal AI on CMR in 16 patients (*Figure 9*). The positive predictive value (PPV) of CMR before PVR was 81% (26/32 patients). Since an abnormal AI on CMR could prompt cryoablation concomitant to surgical PVR or RF ablation before/during transcatheter PVR, EAM, performed solely for diagnostic purposes, could be omitted in all patients with abnormal AI on CMR. For the remaining 16 patients with normal AI on CMR, the negative predictive value (NPV) of CMR was 94% (15/16 patients).

In the remaining 40 patients, who underwent EAM for risk stratification, 23 patients had at least one abnormal AI on CMR, and 17 only had normal AI on CMR (*Figure 9*). The PPV and NPV of CMR were 87% and 100%, respectively. Electroanatomical mapping could be restricted to patients who have abnormal CMR findings with the option to target a SCAI at the time of mapping.

Accordingly, in patients without previous VT or ablation, systematic evaluation by CMR could reduce the need for diagnostic EAM procedures by 74% (EAM is necessary after CMR in 23/88 patients).

Table 4 Performance of previously proposed risk scores for prediction of the presence of slow-conducting anatomical isthmus/blocked anatomical isthmus

	LGE	Median score (IQR)	Odds ratio	95%CI	*P*	AUC
Ghonim 2022[a]	+	23 (12–35)	1.04	.99–1.08	.06	.65
Ghonim without LGE 2022 [a]	–	10 (5–13)	1.05	.98–1.13	.17	.58
Bokma 2017	–	2 (1–3)	1.49	.97–2.31	.06	.68
Khairy without VT inducibility 2008	–	2 (0–4)	1.13	.87–1.48	.35	.56
Babu-Narayan 2006	+	5 (3–6)	1.42	1.00–2.06	.04	.65

AUC, area under the curve; LGE, late gadolinium enhancement.
[a]Data on RVOT akinetic length were not available.

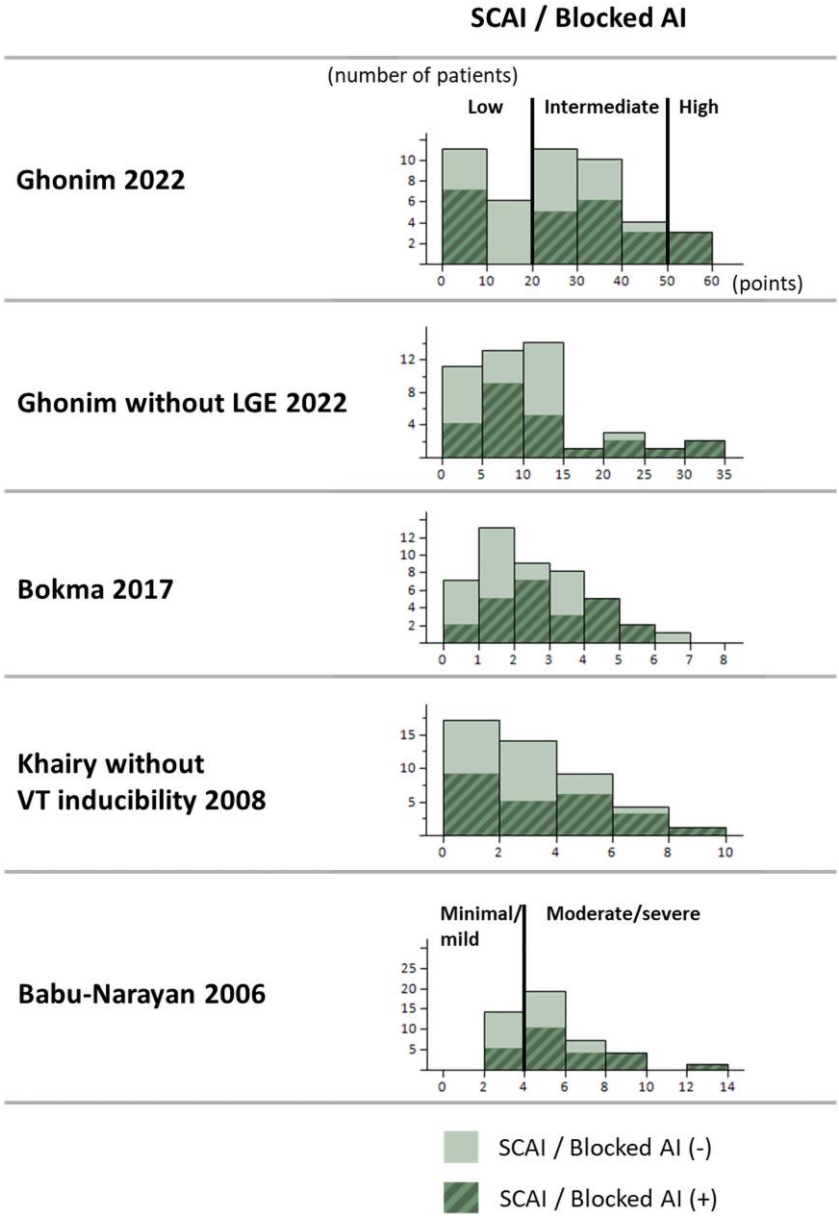

Figure 4 Distribution of patients according to the results of risk scores and presence of slow-conducting anatomical isthmus/blocked anatomical isthmus. AI, anatomical isthmus; LGE, late gadolinium enhancement; SCAI, slow-conducting anatomical isthmus; VT, ventricular tachycardia

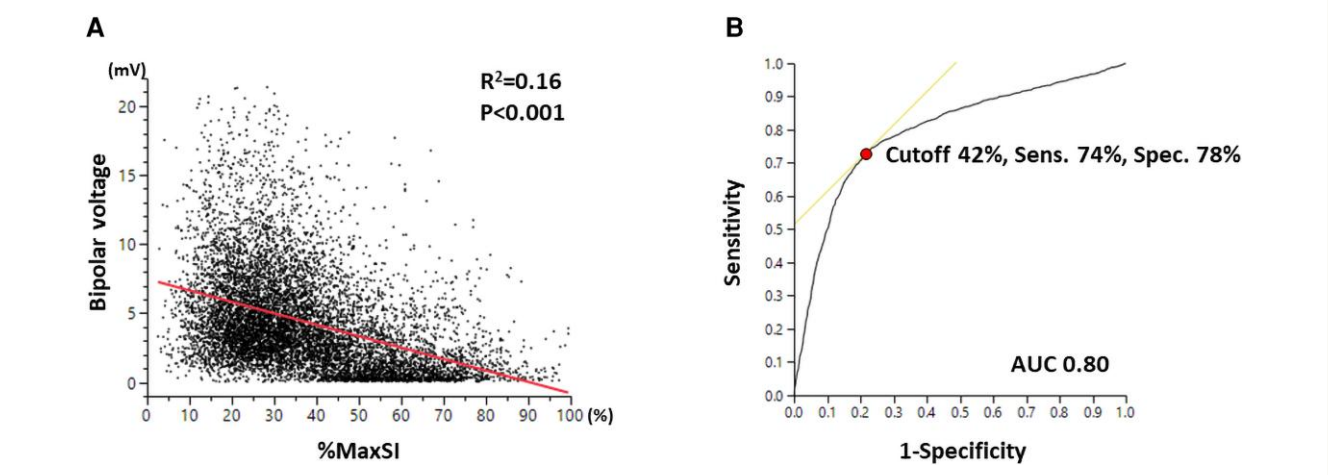

Figure 5 Defining repaired tetralogy of Fallot-specific signal intensity threshold. (*A*) Correlation between bipolar voltage and local signal intensity. (*B*) Receiver operating characteristic analysis for low bipolar voltage correlating to local signal intensity. AUC, area under the curve; BV, bipolar voltage; SI, signal intensity

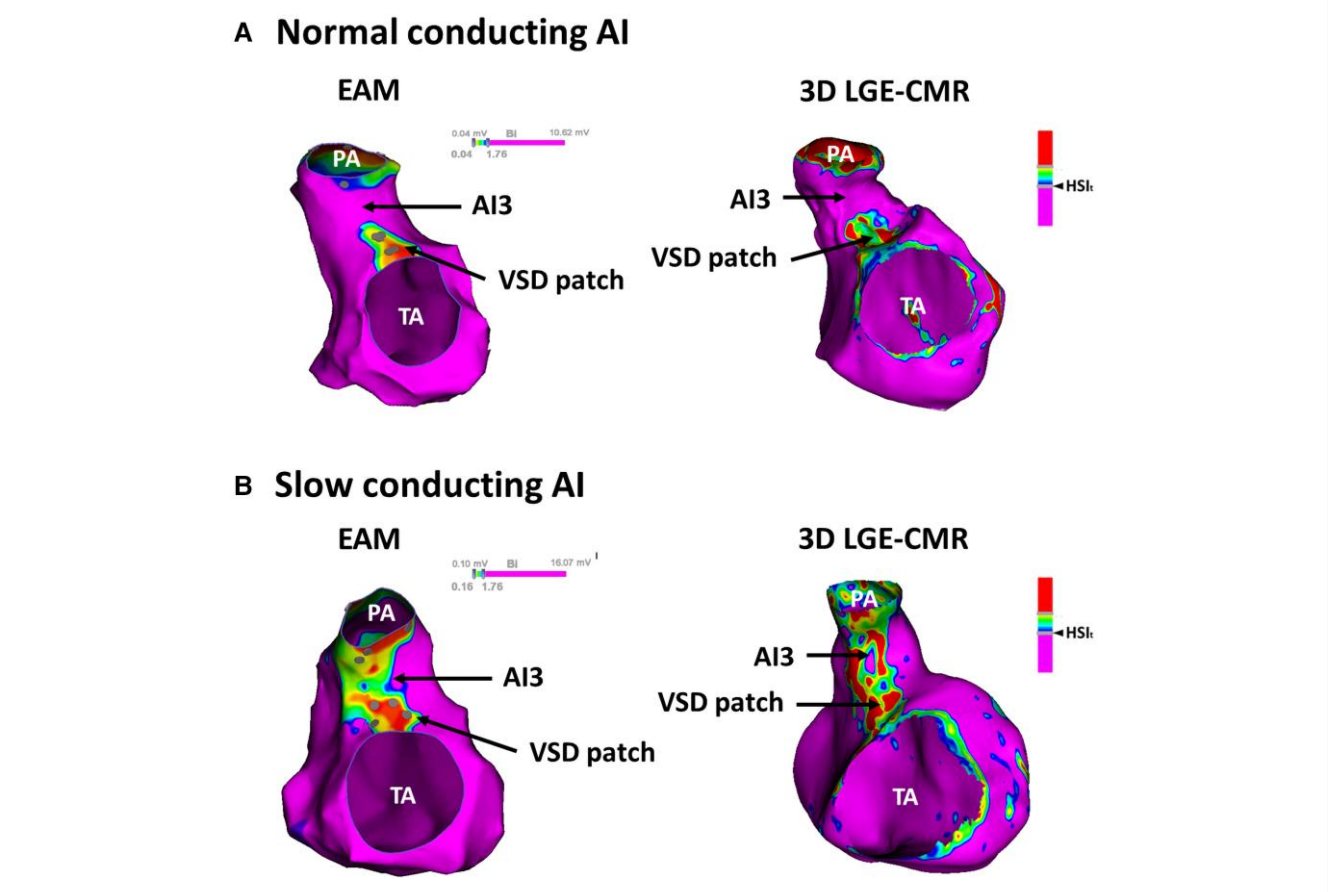

Figure 6 Examples of normal and slow-conducting anatomical isthmuses. (*A*) Normal-conducting anatomical isthmus (left panel) electroanatomical mapping showed normal bipolar voltage within anatomical isthmus 3. Conduction velocity was calculated as 1.1 m/s. (Right panel) 3D late gadolinium enhancement cardiac magnetic resonance represented normal myocardium ($\leq HSI_t$) within anatomical isthmus 3 (normal anatomical isthmus on cardiac magnetic resonance). (*B*) Slow-conducting anatomical isthmus (left panel) electroanatomical mapping showed low bipolar voltage within anatomical isthmus 3. Conduction velocity was calculated as .3 m/s. (Right panel) 3D late gadolinium enhancement cardiac magnetic resonance represented abnormal myocardium ($>HSI_t$) on anatomical isthmus 3 connecting the pulmonary annulus and ventricular septal defect patch (abnormal anatomical isthmus on cardiac magnetic resonance). Signal intensity above HSI_t does detect not only unexcitable tissue but also abnormal myocardium with slow-conducting properties. AI, anatomical isthmus; EAM, electroanatomical mapping; HSI_t, high signal intensity threshold; PA, pulmonary annulus; TA, tricuspid valve annulus; VSD, ventricular septal defect

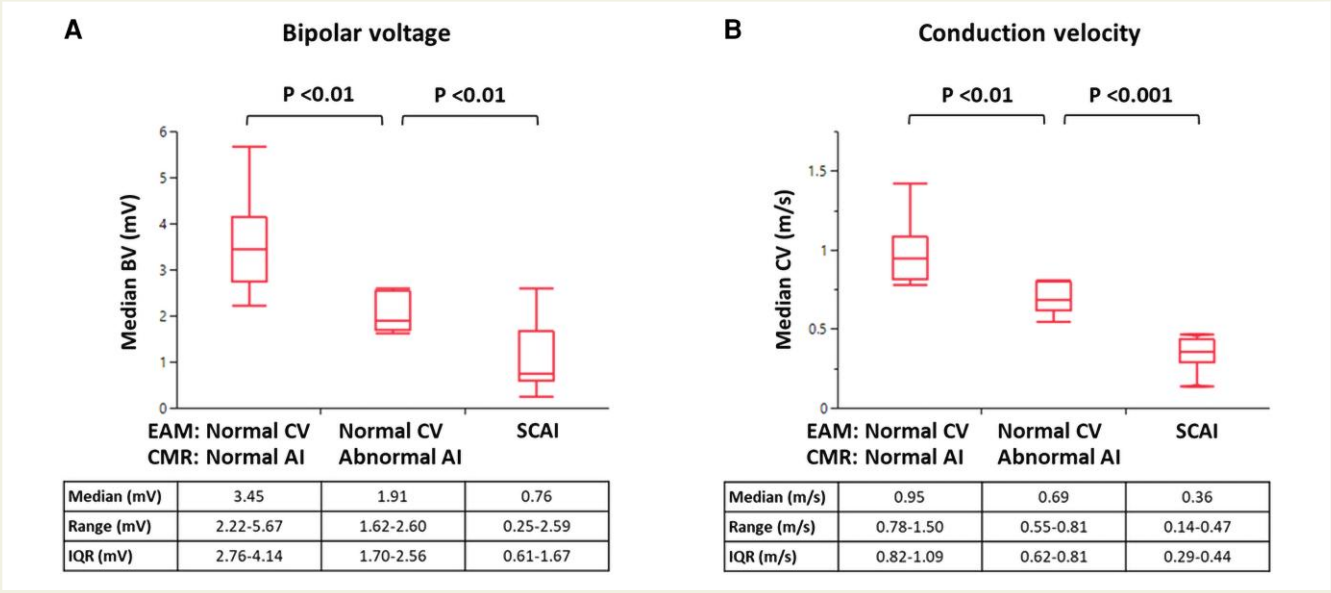

Median (mV)	3.45	1.91	0.76
Range (mV)	2.22-5.67	1.62-2.60	0.25-2.59
IQR (mV)	2.76-4.14	1.70-2.56	0.61-1.67

Median (m/s)	0.95	0.69	0.36
Range (m/s)	0.78-1.50	0.55-0.81	0.14-0.47
IQR (m/s)	0.82-1.09	0.62-0.81	0.29-0.44

Figure 7 Bipolar voltage and conduction velocity of anatomical isthmus 3 according to electroanatomical mapping and cardiac magnetic resonance findings. (*A*) Bipolar voltage. (*B*) Conduction velocity. AI, anatomical isthmus; CMR, cardiac magnetic resonance imaging; CV, conduction velocity; EAM, electroanatomical mapping

Discussion

To the best of our knowledge, this is the first study to demonstrate that 3D-LGE-CMR can non-invasively identify SCAI, the dominant substrate for VT, in patients with rTOF. The newly proposed method of CMR image analysis showed an excellent inter-observer agreement and could identify SCAI or blocked AI with high sensitivity and specificity, which was confirmed in the validation cohort. In addition, compared with patients with NCAI on EAM and normal AI on CMR (true negative CMR), those with NCAI on EAM but abnormal AI on CMR (false-positive CMR) had already significantly lower BV and CV on EAM.

These results suggest that 3D-LGE-CMR can diagnose SCAI with excellent accuracy and may identify a diseased AI3 even before critical conduction delay occurs. This technique can refine patient selection for invasive EAM prior to re-valving and may allow non-invasive and serial testing for the presence of a VT substrate in contemporary patients with rTOF (*Structured Graphical Abstract*).

Slow-conducting anatomical isthmus as the dominant substrate for monomorphic ventricular tachycardia

The vast majority of spontaneous and induced VA in rTOF are re-entrant SMVTs dependent on SCAI.[5,11,16] Among four previously described AIs, AI3 was the most prevalent SCAI in contemporary rTOF patients.[4,5,11,13,17] In line with previous reports, 91% of all SCAI was SCAI3, which was the substrate for all induced VTs in the derivation cohort. Invasive EAM is currently the gold standard to identify SCAI. Of note, repeated mapping may be needed as slow conduction can develop over time (*Figure 8*).

Transection of SCAI by catheter or surgical ablation has been recognized as the most effective, curative, and potentially preventive treatment of SMVT in rTOF.[7,15] Preventive ablation of SCAI3 before PVR is increasingly performed as the abnormal myocardium of AI3 may be covered by the prosthetic materials, becoming inaccessible for future catheter ablation.[8–10] Accordingly, there is a high clinical need for non-invasive identification of SCAI.

In this context, we would like to emphasize that we aimed to non-invasively identify the most prevalent substrate for SMVT. In particular, patients with advanced heart failure and/or a large scar remote from SCAI may have a competing risk to develop non-SCAI-related VA.

Association between risk scores, the presence of slow-conducting anatomical isthmus, and arrhythmogenesis

Risk scores have been developed to predict mortality,[20] ICD shocks,[19] and VA.[21] The occurrence of spontaneous VT depends on the interplay between a pre-existing substrate (SCAI), initiating triggers (e.g. PVCs), and modulating factors including autonomic tone, volume and pressure overload, or heart failure (*Figure 1*). All previously developed risk scores showed an at best moderate performance to discriminate between patients with or without SCAI (AUC < .7) as pre-existing substrate (*Table 4*).

Induction of SMVT by invasive PES, which can be considered as an initiating trigger, proves the presence of a VT substrate. Of interest, risk scores that have included LGE-CMR parameters, namely the extent of LGE and biventricular function (Ghonim 2022 and Babu-Narayan 2006), showed a good and, in general, higher discriminative ability for VT inducibility. However, VT induction is also dependent on modulating factors present at the time of PES that may either facilitate or impede VT inducibility. Therefore, non-inducibility does not exclude the presence of a VT substrate. The poor discriminative ability of the risk scores for SCAI and their better performance for predicting VT inducibility suggest that the outcome of these risk scores is associated with modulators of arrhythmogenesis rather than with the VT substrate.

Extensive myocardial scar detected by LGE-CMR has been also associated with spontaneous VT and SCD in patients with rTOF, supporting the potential value of LGE-CMR.[18,30,31] However, before CMR becomes the decisive factor for risk stratification and for VT substrate

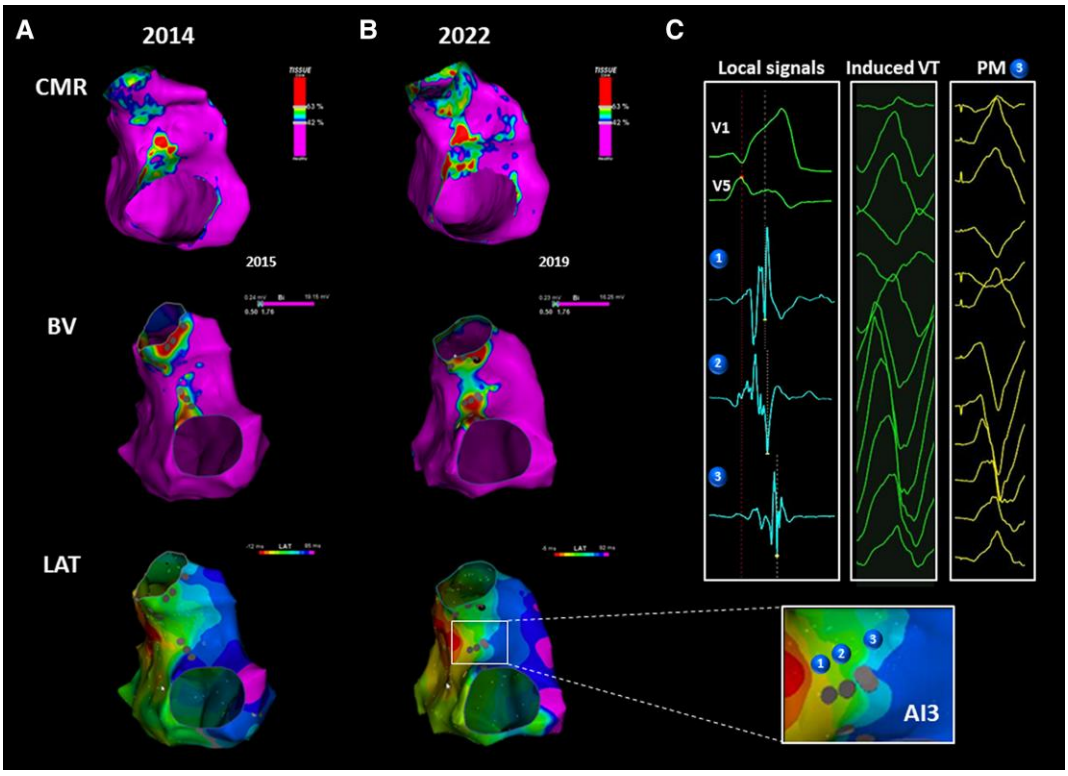

Figure 8 A patient with progression of conduction delay through anatomical isthmus 3. (*A*) The first cardiac magnetic resonance showed narrow (6.3 mm) but normal anatomical isthmus 3. The conduction velocity through the anatomical isthmus 3 was correlated (.81 m/s). (*B*) 3D late gadolinium enhancement cardiac magnetic resonance was repeated 4 years later, showing an abnormal anatomical isthmus 3. Re-electroanatomical mapping was also performed, indicating slow-conducting anatomical isthmus 3. (*C*) Fragmented local signals were observed at slow-conducting anatomical isthmus 3 (Points 1, 2, and 3). Sustained monomorphic ventricular tachycardia was induced and a good pace-match was obtained at slow-conducting anatomical isthmus 3 (point 3). Slow-conducting anatomical isthmus 3 was transected by catheter ablation. AI, anatomical isthmus; CMR, cardiac magnetic resonance imaging; CV, conduction velocity; EAM, electroanatomical mapping; LGE, late gadolinium enhancement; SCAI, slow-conducting anatomical isthmus; SMVT, sustained monomorphic ventricular tachycardia

Table 5 Electroanatomical mapping and cardiac magnetic resonance data of the validation cohort

		Normal AI_{CMR}	Abnormal AI_{CMR}	Total	Sensitivity (95% CI)	Specificity (95% CI)
$AI_{EAM}1$	NCAI	52	0	53	100% (3–100)	100% (93–100)
	SCAI	0	1			
$AI_{EAM}2$	NCAI	7	4	16	100% (48–100)	64% (35–87)
	SCAI	0	5			
$AI_{EAM}3$	NCAI	18	3	53	94% (82–99)	86% (67–96)
	SCAI	2	27			
	Blocked AI	0	3			
$AI_{EAM}4$	NCAI	0	1	2	100% (3–100)	0% (0–98)
	SCAI	0	1			
Total		79	45	124	95% (85–99)	91% (83–96)

See *Table 2* for abbreviations.

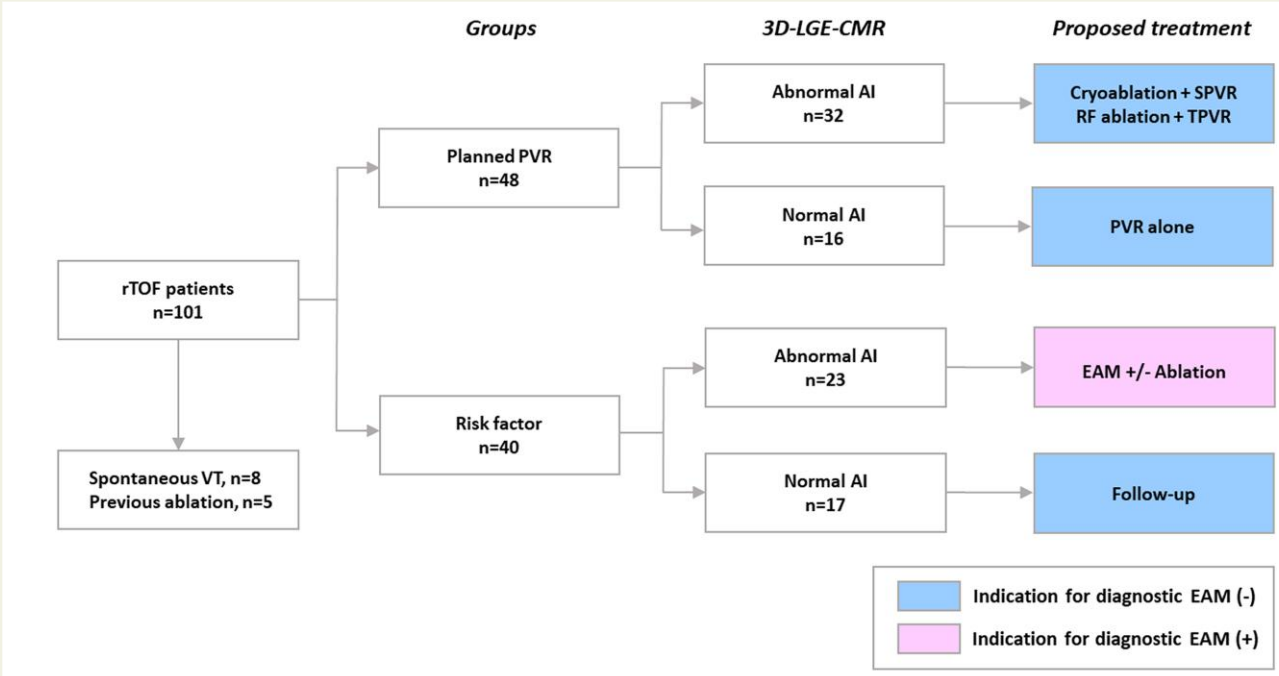

Patients without spontaneous VT or previous ablation (n=88)	3D-LGE CMR		EAM			PPV/NPV of CMR	Proposed treatment
	Finding of AI	Number of pts	NCAI	SCAI	blocked AI		
Pre PVR (n=48)	At least 1 abnormal AI	32[a]	6	26	0	PPV 81%	PVR + ablation
	Only normal AI	16	15	1	0	NPV 94%	PVR alone
Risk stratification (n=40)	At least 1 abnormal AI	23[b]	3	15	5	PPV 87%[c] / 65%[d]	EAM (+ ablation if SCAI+)
	Only normal AI	17	17	0	0	NPV 100%	Follow-up

Figure 9 Impact of systematic evaluation by 3D late gadolinium enhancement cardiac magnetic resonance on patient selection for electroanatomical mapping. The columns 'proposed treatment' are colour corded according to indication for invasive electroanatomical mapping. Blue ($n = 65$): indication for diagnostic electroanatomical mapping (−);red ($n = 23$): indication for diagnostic electroanatomical mapping (+). [a]AI2, $n = 2$; AI3, $n = 24$; AI2 + 3, $n = 5$; AI3 + 4, $n = 1$. [b]AI3, $n = 21$; AI2 + 3, $n = 1$; and AI3 + 4, $n = 1$. [c] PPV for slow-conducting anatomical isthmus/blocked anatomical isthmus. [d]Positive predictive value for slow-conducting anatomical isthmus. AI, anatomical isthmus; CMR, cardiac magnetic resonance imaging; EAM, electroanatomical mapping; NCAI, slow-conducting anatomical isthmus; NPV, negative predictive value; PPV, positive predictive value; RF, radio frequency; SCAI, slow-conducting anatomical isthmus; SPVR, surgical pulmonary valve replacement; TPVR, transcatheter pulmonary valve replacement; VT, ventricular tachycardia

delineation, important aspects need to be considered. First, LGE-CMR methods and SI thresholds to quantify scar and delineate the 3D scar geometry have not been validated for surgical scars and other unexcitable boundaries of AI including endothelialized prosthetic patches. Second, the previous reports have focused on the total LGE burden/volume of the RV with/without LV based on visual assessment of 2D-LGE-CMR or manual segmentation from 3D-LGE-CMR.[18,21,32] The LGE volume has been correlated with VT inducibility, but the significant overlap in LGE values between patients with and without events limits its discriminative value in clinical practice.[32]

Identification of slow-conducting anatomical isthmus by 3D cardiac magnetic resonance

The feasibility of semi-automated scar segmentation from 3D-LGE-CMR has been reported in a small series of rTOF patients.[22] The 3D imaging technique is especially useful for morphologically complex architectures, such as the RVOT, where the 2D technique cannot maintain continuously co-axial slices to the imaging plane, increasing partial volume effects.[22] Annotation of the mid-myocardial layer allows the exclusion of a high-intensity signal from the blood pool and does not exclude patch materials, which appear as a transmural high-intensity lesion.

In the present study, we performed reversed registration of CMR and EAM data allowing the direct comparison of BV on EAM with the local SI. The obtained AUC (.8) was similar or superior to the values reported in acquired heart diseases.[33] We identified 42% of maxSI as the best SI cut-off for abnormal myocardium, which, when continuously present between anatomical boundaries, was consistent with slow-conducting or blocked AI during EAM. The excellent sensitivity and specificity of 3D-LGE-CMR for SCAI were confirmed in the large validation cohort. In the two false-negative CMRs in the validation cohort, the automatically determined area with maximal SI was incorrect, which can be easily, manually controlled and adjusted (see Supplementary data online, *Figure S2*). Importantly, most patients in the validation

cohort were from an independent centre, with different CMR scanners and protocols used. This further supports the generalizability of the approach.

Slow-conducting anatomical isthmus cannot be differentiated from a blocked AI by CMR. However, a pre-existing blocked AI is rare, observed in only 4.6% of patients in our cohort. Human studies have demonstrated that slow conduction can occur even through single myocardial bundles with a diameter of 200 μm. The current resolution of *in vivo* LGE-CMRs does not allow the detection of single bundles, which may explain the inability to distinguish between SCAI and blocked AI.[34]

Late gadolinium enhancement cardiac magnetic resonance for early detection of adverse remodelling

There is a time-dependent risk of life-threatening VT in rTOF.[35] Adverse remodelling and slow conduction across AI may develop over time. In the present study, one patient who underwent repeated EAM and CMR showed voltage reduction and progressive conduction delay across AI3 over 4 years, correctly identified by CMR.

3D-LGE-CMR may even identify AI3 that are more likely to remodel over time before critical conduction delay occurs. The six patients with false-positive CMR finding had already significantly lower BV and CV than those with true positive CMR finding.

Potential impact of systematic evaluation by cardiac magnetic resonance on indication for electroanatomical mapping in patients without spontaneous ventricular tachycardia or previous ablation

The excellent NPV of the 3D-LGE-CMR for SCAI impacts the need for invasive EAM, currently performed for risk stratification and before re-valving. Systematic evaluation by CMR would indeed significantly reduce diagnostic EAM procedures (*Figure 9*), following the proposed approach.

Particularly in patients before PVR, abnormal AI on CMR could prompt cryoablation concomitant to surgical PVR and RF ablation before/during transcatheter PVR, without prior diagnostic EAM.[15,36] The PPV for SCAI of abnormal AI on CMR is high (81%) and even 'false-positive CMR' correlated with borderline BV and CV reduction. Conduction velocity in these AI may further slow due to aging and/or the intervention and may become inaccessible after PVR.[9,10] Although data to support the ablation of AI with borderline properties are currently lacking, it may be reasonable to intraoperatively target narrow AI with borderline CV reduction, considering the fast surgical procedure without reported complications.[12–14]

In patients followed for risk stratification, EAM can be combined with catheter ablation of the AI during the same procedure, if a SCAI is likely based on serial CMR.

Limitations

The patients included in this study were referred for EAM before re-valving, for risk stratification, or treatment of spontaneous VT, and the findings may not be generalizable to all rTOF patients. Follow-up studies are required to evaluate if LGE-CMR can detect AI that will develop slow conduction over time, thereby justifying preventive ablation based on LGE-CMR only in those who are scheduled for re-valving.

The acquisition of 3D-LGE-CMR requires expertise and has a substantial learning curve. The availability of ADAS-3D image post-processing software may be limited. However, patients with congenital heart disease are more gathered to tertiary centres where a variety of imaging software is deployed. Our novel concept and required methods may be adopted by other software packages.

In only two cases, CMR analysis did not detect a SCAI (false-negative CMR), which may be due to an incorrect selection of the automatically determined area of maxSI. Visual control of automatically set reference areas may overcome this problem.

Not all variables were available for all patients, as most patients were included retrospectively.

Although multipolar catheters may facilitate fast acquisition of BV and LAT, the use of a single ablation catheter for mapping with reliable catheter-tissue contact may be of advantage to evaluate non-excitable tissue and allow for immediate treatment without additional costs.

Conclusion

3D late gadolinium enhancement cardiac magnetic resonance can identify SCAI with excellent diagnostic accuracy and may identify diseased AI even before critical conduction delay occurs. This technique can refine patient selection for invasive EAM and may allow for non-invasive and serial VT substrate identification and risk stratification for life-threatening VT.

Acknowledgements

The authors would like to sincerely thank Prof Dr William G. Stevenson (Vanderbilt University Medical Center, TN, USA) for his insightful comments.

Supplementary data

Supplementary data are available at *European Heart Journal* online.

Declarations

Disclosure of Interest

No disclosures related to the manuscript. The Department of Cardiology receives investigator-initiated research grants from Biosense Webster.

Data Availability

To maintain patient confidentiality, data and study materials will not be made available to other researchers for the purposes of replicating the results.

Funding

We acknowledge the support from the Netherlands Cardiovascular Research Initiative: An initiative with support of the Dutch Heart Foundation and Hartekind, CVON2019–002 OUTREACH.

Ethical Approval

For the retrospective part, the Medical Ethics Committee (METC Leiden Den Haag Delft) waived the need for written informed consent,

as all data were acquired according to routine clinical care. The prospective registry was approved by the METC (G21.137).

Pre-registered Clinical Trial Number

None supplied.

References

1. Marelli AJ, Mackie AS, Ionescu-Ittu R, Rahme E, Pilote L. Congenital heart disease in the general population: changing prevalence and age distribution. *Circulation* 2007;**115**:163–72. https://doi.org/10.1161/CIRCULATIONAHA.106.627224
2. Marelli AJ, Ionescu-Ittu R, Mackie AS, Guo L, Dendukuri N, Kaouache M. Lifetime prevalence of congenital heart disease in the general population from 2000 to 2010. *Circulation* 2014;**130**:749–56. https://doi.org/10.1161/CIRCULATIONAHA.113.008396
3. Zeppenfeld K, Schalij MJ, Bartelings MM, Tedrow UB, Koplan BA, Soejima K, *et al.* Catheter ablation of ventricular tachycardia after repair of congenital heart disease: electroanatomic identification of the critical right ventricular isthmus. *Circulation* 2007;**116**:2241–52. https://doi.org/10.1161/CIRCULATIONAHA.107.723551
4. Moore JP, Seki A, Shannon KM, Mandapati R, Tung R, Fishbein MC. Characterization of anatomic ventricular tachycardia isthmus pathology after surgical repair of tetralogy of Fallot. *Circ Arrhythm Electrophysiol* 2013;**6**:905–11. https://doi.org/10.1161/CIRCEP.113.000450
5. Kapel GF, Sacher F, Dekkers OM, Watanabe M, Blom NA, Thambo J-B, *et al.* Arrhythmogenic anatomical isthmuses identified by electroanatomical mapping are the substrate for ventricular tachycardia in repaired Tetralogy of Fallot. *Eur Heart J* 2017;**38**:268–76. https://doi.org/10.1093/eurheartj/ehw202
6. Yang J, Brunnquell M, Liang JJ, Callans DJ, Garcia FC, Lin D, *et al.* Long term follow-up after ventricular tachycardia ablation in patients with congenital heart disease. *J Cardiovasc Electrophysiol* 2019;**30**:1560–8. https://doi.org/10.1111/jce.13996
7. Kapel GF, Reichlin T, Wijnmaalen AP, Piers SR, Holman ER, Tedrow UB, *et al.* Re-entry using anatomically determined isthmuses: a curable ventricular tachycardia in repaired congenital heart disease. *Circ Arrhythm Electrophysiol* 2015;**8**:102–9. https://doi.org/10.1161/CIRCEP.114.001929
8. Kapel GFL, Reichlin T, Wijnmaalen AP, Tedrow UB, Piers SR, Schalij MJ, *et al.* Left-sided ablation of ventricular tachycardia in adults with repaired tetralogy of Fallot: a case series. *Circ Arrhythm Electrophysiol* 2014;**7**:889–97. https://doi.org/10.1161/CIRCEP.114.001661
9. Moore JP, Aboulhosn JA, Zeppenfeld K, Waldmann V, Bessiere F, Blom NA, *et al.* Rationale and design of the multicenter catheter ablation of ventricular tachycardia before transcatheter pulmonary valve replacement in repaired tetralogy of Fallot study. *Am J Cardiol* 2023;**204**:14–21. https://doi.org/10.1016/j.amjcard.2023.07.087
10. Moore JP, Aboulhosn JA, Khairy P. Electrophysiology testing before transcatheter pulmonary valve replacement in patients with repaired tetralogy of Fallot. *Eur Heart J* 2023;**44**:3228–30. https://doi.org/10.1093/eurheartj/ehad483
11. Waldmann V, Bessiere F, Gardey K, Bakloul M, Belli E, Bonnet D, *et al.* Systematic electrophysiological study prior to pulmonary valve replacement in tetralogy of Fallot: a prospective multicenter study. *Circ Arrhythm Electrophysiol* 2023;**16**:e011745. https://doi.org/10.1161/CIRCEP.122.011745
12. Nevvazhay T, Zeppenfeld K, Brouwer C, Hazekamp M. Intraoperative cryoablation in late pulmonary valve replacement for tetralogy of Fallot. *Interact Cardiovasc Thorac Surg* 2020;**30**:780–2. https://doi.org/10.1093/icvts/ivaa013
13. Bouyer B, Jalal Z, Daniel Ramirez F, Derval N, Iriart X, Duchateau J, *et al.* Electrophysiological study prior to planned pulmonary valve replacement in patients with repaired tetralogy of Fallot. *J Cardiovasc Electrophysiol* 2023;**34**:1395–404. https://doi.org/10.1111/jce.15940
14. Sandhu A, Ruckdeschel E, Sauer WH, Collins KK, Kay JD, Khanna A, *et al.* Perioperative electrophysiology study in patients with tetralogy of Fallot undergoing pulmonary valve replacement will identify those at high risk of subsequent ventricular tachycardia. *Heart Rhythm* 2018;**15**:679–85. https://doi.org/10.1016/j.hrthm.2018.01.020
15. Zeppenfeld K, Tfelt-Hansen J, de Riva M, Winkel BG, Behr ER, Blom NA, *et al.* 2022 ESC guidelines for the management of patients with ventricular arrhythmias and the prevention of sudden cardiac death. *Eur Heart J* 2022;**43**:3997–4126. https://doi.org/10.1093/eurheartj/ehac262
16. Bessiere F, Waldmann V, Combes N, Metton O, Dib N, Mondesert B, *et al.* Ventricular arrhythmias in adults with congenital heart disease, part I: JACC State-of-the-Art Review. *J Am Coll Cardiol* 2023;**82**:1108–20. https://doi.org/10.1016/j.jacc.2023.06.034
17. Moore JP, Shannon KM, Khairy P, Waldmann V, Bessiere F, Burrows A, *et al.* Sinus rhythm QRS morphology reflects right ventricular activation and anatomical ventricular tachycardia isthmus conduction in repaired tetralogy of Fallot. *Heart Rhythm* 2023;**20**:1689–96. https://doi.org/10.1016/j.hrthm.2023.08.020
18. Babu-Narayan SV, Kilner PJ, Li W, Moon JC, Goktekin O, Davlouros PA, *et al.* Ventricular fibrosis suggested by cardiovascular magnetic resonance in adults with repaired tetralogy of Fallot and its relationship to adverse markers of clinical outcome. *Circulation* 2006;**113**:405–13. https://doi.org/10.1161/CIRCULATIONAHA.105.548727
19. Khairy P, Harris L, Landzberg MJ, Viswanathan S, Barlow A, Gatzoulis MA, *et al.* Implantable cardioverter-defibrillators in tetralogy of Fallot. *Circulation* 2008;**117**:363–70. https://doi.org/10.1161/CIRCULATIONAHA.107.726372
20. Bokma JP, Winter MM, Vehmeijer JT, Vliegen HW, van Dijk AP, van Melle JP, *et al.* QRS fragmentation is superior to QRS duration in predicting mortality in adults with tetralogy of Fallot. *Heart* 2017;**103**:666–71. https://doi.org/10.1136/heartjnl-2016-310068
21. Ghonim S, Gatzoulis MA, Ernst S, Li W, Moon JC, Smith GC, *et al.* Predicting survival in repaired tetralogy of Fallot: a lesion-specific and personalized approach. *JACC Cardiovasc Imaging* 2022;**15**:257–68. https://doi.org/10.1016/j.jcmg.2021.07.026
22. Stirrat J, Rajchl M, Bergin L, Patton DJ, Peters T, White JA. High-resolution 3-dimensional late gadolinium enhancement scar imaging in surgically corrected tetralogy of Fallot: clinical feasibility of volumetric quantification and visualization. *J Cardiovasc Magn Reson* 2014;**16**:76. https://doi.org/10.1186/s12968-014-0076-y
23. Nagueh SF, Appleton CP, Gillebert TC, Marino PN, Oh JK, Smiseth OA, *et al.* Recommendations for the evaluation of left ventricular diastolic function by echocardiography. *J Am Soc Echocardiogr* 2009;**22**:107–33. https://doi.org/10.1016/j.echo.2008.11.023
24. Aboulhosn JA, Lluri G, Gurvitz MZ, Khairy P, Mongeon FP, Kay J, *et al.* Left and right ventricular diastolic function in adults with surgically repaired tetralogy of Fallot: a multi-institutional study. *Can J Cardiol* 2013;**29**:866–72. https://doi.org/10.1016/j.cjca.2012.11.003
25. Bizino MB, Tao Q, Amersfoort J, Siebelink HJ, van den Bogaard PJ, van der Geest RJ, *et al.* High spatial resolution free-breathing 3D late gadolinium enhancement cardiac magnetic resonance imaging in ischaemic and non-ischaemic cardiomyopathy: quantitative assessment of scar mass and image quality. *Eur Radiol* 2018;**28**:4027–35. https://doi.org/10.1007/s00330-018-5361-y
26. Kapel GFL, Brouwer C, Jalal Z, Sacher F, Venlet J, Schalij MJ, *et al.* Slow conducting electroanatomic isthmuses: an important link between QRS duration and ventricular tachycardia in tetralogy of Fallot. *JACC Clin Electrophysiol* 2018;**4**:781–93. https://doi.org/10.1016/j.jacep.2018.02.002
27. Zeppenfeld K, Kimura Y. Catheter ablation of ventricular tachycardia in congenital heart disease, editors. *Catheter Ablation of Cardiac Arrhythmias in Children and Patients with Congenital Heart Disease*. Boca Raton, Florida: CRC Press; 2021. p238–54.
28. Rivas-Gandara N, Dos-Subira L, Francisco-Pascual J, Rodriguez-Garcia J, Pijuan-Domenech A, Benito B, *et al.* Substrate characterization of right ventricle in repaired tetralogy of Fallot using late enhancement cardiac magnetic resonance. *Heart Rhythm* 2021;**18**:1868–75. https://doi.org/10.1016/j.hrthm.2021.05.032
29. Teijeira-Fernandez E, Cochet H, Bourier F, Takigawa M, Cheniti G, Thompson N, *et al.* Influence of contact force on voltage mapping: a combined magnetic resonance imaging and electroanatomic mapping study in patients with tetralogy of Fallot. *Heart Rhythm* 2018;**15**:1198–205. https://doi.org/10.1016/j.hrthm.2018.03.022
30. Baumgartner H, Backer D, Babu-Narayan J, Budts SV, Chessa W, Diller M, *et al.* 2020 ESC guidelines for the management of adult congenital heart disease. *Eur Heart J* 2021;**42**:563–645. https://doi.org/10.1093/eurheartj/ehaa554
31. Stout KK, Daniels CJ, Aboulhosn JA, Bozkurt B, Broberg CS, Colman JM, *et al.* 2018 AHA/ACC guideline for the management of adults with congenital heart disease: a report of the American College of Cardiology/American Heart Association Task Force on Clinical Practice Guidelines. *Circulation* 2019;**139**:e698–800. https://doi.org/10.1161/CIR.0000000000000603
32. Ghonim S, Ernst S, Keegan J, Giannakidis A, Spadotto V, Voges I, *et al.* Three-dimensional late gadolinium enhancement cardiovascular magnetic resonance predicts inducibility of ventricular tachycardia in adults with repaired tetralogy of Fallot. *Circ Arrhythm Electrophysiol* 2020;**13**:e008321. https://doi.org/10.1161/CIRCEP.119.008321
33. Piers SR, Tao Q, van Huls van Taxis CF, Schalij MJ, van der Geest RJ, Zeppenfeld K. Contrast-enhanced MRI-derived scar patterns and associated ventricular tachycardias in nonischemic cardiomyopathy: implications for the ablation strategy. *Circ Arrhythm Electrophysiol* 2013;**6**:875–83. https://doi.org/10.1161/CIRCEP.113.000537
34. de Bakker JM, van Capelle FJ, Janse MJ, Tasseron S, Vermeulen JT, de Jonge N, *et al.* Slow conduction in the infarcted human heart. 'Zigzag' course of activation. *Circulation* 1993;**88**:915–26. https://doi.org/10.1161/01.CIR.88.3.915
35. Khairy P, Aboulhosn J, Gurvitz MZ, Opotowsky AR, Mongeon FP, Kay J, *et al.* Arrhythmia burden in adults with surgically repaired tetralogy of Fallot: a multi-institutional study. *Circulation* 2010;**122**:868–75. https://doi.org/10.1161/CIRCULATIONAHA.109.928481
36. Krieger EV, Zeppenfeld K, DeWitt ES, Duarte VE, Egbe AC, Haeffele C, *et al.* Arrhythmias in repaired tetralogy of fallot: a scientific statement from the American Heart Association. *Circ Arrhythm Electrophysiol* 2022;**15**:e000084. https://doi.org/10.1161/HAE.0000000000000084